AGU PUBLICATIONS

JGR

Journal of Geophysical Research: Space Physics

RESEARCH ARTICLE

10.1002/2013JA019522

Key Points:
- An ICME can cause compression of the Mars ionosphere
- An ICME can cause the Mars ionosphere to oscillate
- An ICME causes extension of the Mars ionosphere and possible loss of atmospheric material

Correspondence to:
D. D. Morgan,
david-morgan@uiowa.edu

Citation:
Morgan, D. D., et al. (2014), Effects of a strong ICME on the Martian ionosphere as detected by Mars Express and Mars Odyssey, *J. Geophys. Res. Space Physics*, *119*, doi:10.1002/2013JA019522.

Received 9 OCT 2013
Accepted 29 JUN 2014
Accepted article online 1 JUL 2014

Effects of a strong ICME on the Martian ionosphere as detected by Mars Express and Mars Odyssey

D. D. Morgan[1], C. Diéval[1], D. A. Gurnett[1], F. Duru[1], E. M. Dubinin[2], M. Fränz[2], D. J. Andrews[3], H. J. Opgenoorth[3], D. Uluşen[4], I. Mitrofanov[5], and J. J. Plaut[6]

[1]Department of Physics and Astronomy, University of Iowa, Iowa City, Iowa, USA, [2]Max Planck Institute for Solar System Research, Katlenburg-Lindau, Germany, [3]Swedish Space Science Institute, Uppsala, Sweden, [4]Space Technologies Research Institute, Ankara, Turkey, [5]Space Sciences Institute, Russian Academy of Sciences, Moscow, Russia, [6]Jet Propulsion Laboratory, California Institute of Technology, Pasadena, California, USA

Abstract We present evidence of a substantial ionospheric response to a strong interplanetary coronal mass ejection (ICME) detected by the Mars Advanced Radar for Subsurface and Ionosphere Sounding (MARSIS) on board the Mars Express (MEX) spacecraft. A powerful ICME impacted the Martian ionosphere beginning on 5 June 2011, peaking on 6 June, and trailing off over about a week. This event caused a strong response in the charged particle detector of the High-Energy Neutron Detector (HEND) on board the Odyssey spacecraft. The ion mass spectrometer of the Analyzer of Space Plasmas and Energetic Atoms instrument on MEX detected an increase in background counts, simultaneous with the increase seen by HEND, due to the flux of solar energetic particles (SEPs) associated with the ICME. Local densities and magnetic field strengths measured by MARSIS and enhancements of 100 eV electrons denote the passing of an intense space weather event. Local density and magnetosheath electron measurements and remote soundings show compression of ionospheric plasma to lower altitudes due to increased solar wind dynamic pressure. MARSIS topside sounding of the ionosphere indicates that it is extended well beyond the terminator, to about 116° solar zenith angle, in a highly disturbed state. This extension may be due to increased ionization due to SEPs and magnetosheath electrons or to plasma transport across the terminator. The surface reflection from both ionospheric sounding and subsurface modes of the MARSIS radar was attenuated, indicating increased electron content in the Mars ionosphere at low altitudes, where the atmosphere is dense.

1. Introduction

There is a strong scientific interest in both the current state and the evolution of the atmosphere and ionosphere of Mars. The motivation for the intense interest in this subject is developed in the pages dedicated to it in the most recent Decadal Survey [*Committee on the Planetary Science Decadal Survey Space Studies Board*, 2011a, 2011b]. An essential part of the evolution of the Martian atmosphere is the question of whether and how loss of atmospheric material, especially the constituents of water, occurred over the evolution of the planet and continues to occur in the present era. There are many ways in which atoms and ions can be removed from the Martian atmosphere, for example, sputtering, charge exchange, ion pickup [see, e.g., *Dubinin et al.*, 2011]. These processes can be exacerbated by space weather events, such as corotating interaction regions (CIRs) and coronal mass ejections (CMEs) [*Dubinin et al.*, 2009; *Edberg et al.*, 2010], as well as solar energetic particles (SEPs) [*Futaana et al.*, 2008]. CMEs are thought to be flux-rope-like plasma structures emitted from the Sun [*Forbes et al.*, 2006] that often generate shocks [*Vourlidas et al.*, 2013] and that often occur in association with solar flares. Interplanetary shocks have long been known to accelerate particles to MeV energies [see, e.g., *Sarris and Allen*, 1974; *Krimigis and Venkatesan*, 1988; *Krimigis*, 1992]. Figure 12 of *Krimigis* [1992] shows clear particle acceleration by an interplanetary shock. When CMEs propagate through the interplanetary medium, or solar wind, they are referred to as interplanetary coronal mass ejections (ICMEs).

In this work, we shall discuss a single case where interaction of the Martian ionosphere with a strong ICME was directly observed using the Mars Advanced Radar for Subsurface and Ionosphere Sounding (MARSIS) and Analyzer of Space Plasmas and Energetic Atoms (ASPERA-3) on board the Mars Express (MEX) spacecraft, and the High-Energy Neutron Detector (HEND) on board the Mars Odyssey spacecraft, both in orbit around Mars.

The study of atmospheric loss has in recent years been pursued at both Venus and Mars, whose atmospheres and ionospheres have in common the lack of a global magnetic field, although the discovery of localized remanent magnetic fields embedded in the crust of Mars [*Acuña et al.*, 2001] makes the Martian ionosphere the more complicated of the two. (As an example of this increased complexity, see *Andrews et al.* [2013], where contrasting dayside and nightside effects of the remanent fields are identified.) The key to making observations of atmospheric loss at Venus and Mars are the near-identical ASPERA-3 and ASPERA-4 instruments deployed on the Mars Express and Venus Express (VEX) spacecraft [*Lundin et al.*, 2008, 2009; *Barabash et al.*, 2006]. Observations of an ICME interaction with Venus have been reported, for example, by *McEnulty et al.* [2010], who noted the intensification of solar wind-ionosphere interactions at Venus during the interaction with an ICME using ASPERA-4. These authors found a clear energization due to pickup by the increased convection electric field of an ICME, but the flux of particles lost to the solar wind was not clearly affected.

Some of our best information about the interaction of the Martian environment with space weather events comes from observations made with the Mars Global Surveyor (MGS)0 spacecraft during the Halloween superstorm of 2003. *Crider et al.* [2005] noted strong compression of the ionosphere during the ICME based on the magnetic field proxy measurement for dynamic pressure of *Crider et al.* [2003]. The theme of a pressure pulse leading to ion loss from the Martian ionosphere is taken up by *Edberg et al.* [2010] in a statistical study that confirms the findings of previous case studies: pressure pulses, whether from CIRs or ICMEs, lead to an increase in ions lost from the planet.

Space weather at Mars has also been studied by *Uluşen et al.* [2012]. These authors used MGS radio occultation results taken during SEP events to show that effects on the electron density are not related in a clear or obvious way to influx of either protons or electrons. They observed no clear evidence for an ionospheric density increase between 100 and 200 km altitudes and proposed that one possible reason for this may be the extra ionization produced by SEPs is below 80 km, out of the range of radio science profiles. Moreover, in a few cases, they noticed a sharp reduction in the electron density of the M1 layer, 30 km or so below the peak of the main (M2) ionospheric layer, during strong SEP events. Energy absorption at varying altitude for different energies appears to be responsible for some of these anomalous effects. *Uluşen et al.* [2012] also notice effects that appear to be due to compression of the ionosphere, a recurring theme in this research.

More recently, *Opgenoorth et al.* [2013] have discussed in detail effects apparent in the ASPERA-3 and MARSIS Active Ionospheric Sounding (AIS) local density measurements for three space weather events seen at Mars that were also detected at Earth due to Sun-Earth-Mars conjunction. These events, which occurred during March and April of 2010, consisted of a corotating interaction region (CIR), a second CIR possibly coupled with a small ICME, and a more substantial ICME that, however, dealt the Martian ionosphere only a glancing blow. These authors note the aforementioned compression of the ionosphere coupled with energization of heavy ions in the magnetosheath.

From this brief review of the literature on solar wind interaction with the Martian ionosphere, we note the recurring themes of ionospheric compression and energization concurrent with the impact of the ICME. In at least one case, the excitation of ionospheric oscillation was noted. These themes shall all be reiterated in the present work. We shall expand on these themes with data not previously invoked to illuminate these phenomena and we shall report additional effects on the Martian ionosphere, not previously noted.

This paper is divided into five sections: first, this introduction; second, brief descriptions of the MARSIS, ASPERA-3, and HEND instruments and their data; third, observations during a strong ICME event from these instruments; fourth, interpretation of those observations, and finally a brief summary.

2. MARSIS AIS, ASPERA-3, and HEND Instruments and Data

The MARSIS radar, on board the MEX spacecraft, is a low-frequency radar with two modes of operation: Subsurface Sounding and Active Ionospheric Sounding (AIS). MARSIS consists of an antenna, 40 m tip to tip, with associated radio transmitter, receiver, and digital processing system [*Picardi et al.*, 2004; *Jordan et al.*, 2009]. In AIS mode, the operation is that of a simple swept-frequency radar sounder, as described by *Franklin and Maclean* [1969]. There are 160 frequencies chosen from 0.1 to 5.5 MHz with roughly logarithmic spacing.

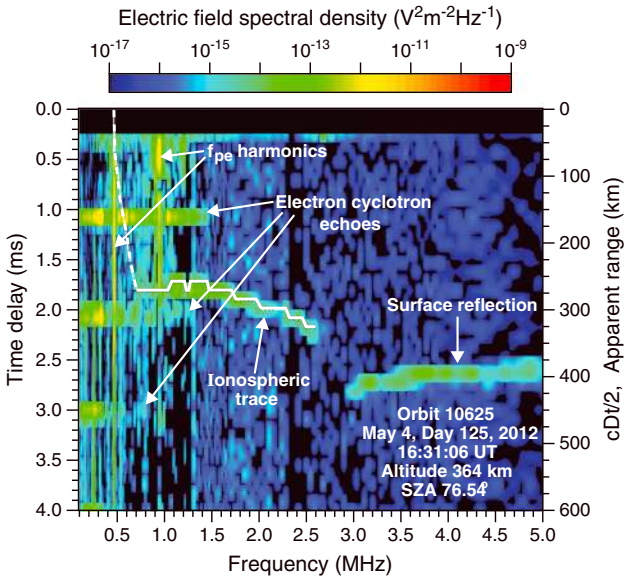

Figure 1. Sample ionogram showing measurable data objects.

A sounding pulse is transmitted in a dipole pattern at the chosen frequency for a duration of 91.4 μs, with a bandwidth of 10.9 kHz. The instrument is then switched to "receive" mode 254 μs after the transmission for 80 time intervals of 91.4 μs each. The transmit-receive cycle at a given frequency lasts for 7.86 ms. After the completion of such a cycle, the frequency is switched to the next higher sample frequency and the cycle is repeated. Taking data for all 160 frequencies takes 1.26 s. When this cycle is complete, the instrument is dormant for five periods of 1.26 s, after which the process is repeated. The intensity data taken in 1.26 s can be represented as a plot of received spectral intensity as a function of the sounding frequency and delay time. An example of such a plot, called an ionogram, is shown in Figure 1. When the instrument is operating, it collects an ionogram's worth of data every 7.54 s. The AIS component of the MARSIS data is described in more detail by *Morgan et al.* [2013a]. Initial results from ionospheric sounding are summarized by *Gurnett et al.* [2005, 2008].

Figure 1 shows four objects of measurement that MARSIS AIS can capture: the ionospheric reflection, the surface reflection, the local plasma frequency, and the local electron cyclotron period. The processes for capturing and processing the ionospheric trace are explained in detail by *Morgan et al.* [2008, 2013a]. The plasma frequency harmonics and their relation to the electron density were first noted by *Gurnett et al.* [2005]. Collection of the local electron density from the electron plasma frequency harmonics (low-frequency vertical lines in the upper left of Figure 1) is explained in detail by *Duru et al.* [2008] and *Morgan et al.* [2013a]. (An automated method for analyzing the local electron density data is described by *Andrews et al.* [2013].) The former reference also explains that the local electron density is not measurable in the magnetosheath or solar wind because the plasma oscillations are convected away from the spacecraft by the bulk velocity, a fact that will be of interest later. Determination of the local magnetic field strength is explained by *Gurnett et al.* [2005, 2008] and *Akalin et al.* [2010]. The average visibility of the surface reflection was used by *Morgan et al.* [2006, 2010] as an indicator of ionospheric absorption from enhanced electron density during solar energetic particle (SEP) storms.

All four of these measurements are employed in the present work. Effects of the ICME will be seen in the local plasma frequency, the local magnetic field strength, the surface reflection, the peak ionospheric electron density, and the electron density profile derived from the ionospheric trace. We shall make use of the apparent altitude and electron density profiles from radar remote sensing. Finally, we shall use the MARSIS subsurface surface reflection as a qualitative indicator of the electron content of the ionosphere, as was done by *Espley et al.* [2007].

This paper also uses data from ASPERA-3, on board MEX [see *Barabash et al.*, 2004]. This instrument includes an Electron Spectrometer (ELS) and an Ion Mass Analyzer (IMA), which we describe briefly below.

The Electron Spectrometer, ELS, consists of a collimator system, an electrostatic top-hat analyzer to select the electrons by energy, and a microchannel plate detector. It measures electrons within a field of view of 4° × 360°, divided into 16 sectors. In this study, ELS sweeps through 128 logarithmically spaced energy steps between 0.4 eV and 20 keV at a 4 s time resolution and an energy resolution of 8%. The observation of low energy electrons is prevented by a −5 V grid voltage.

The Ion Mass Analyzer, IMA, consists of an electrostatic deflection system to select the ions by polar angle, an electrostatic top-hat analyzer to select the ions by energy per unit charge, a permanent magnet-based deflection system to separate the ion masses, and a microchannel plate detector. IMA sweeps through 96

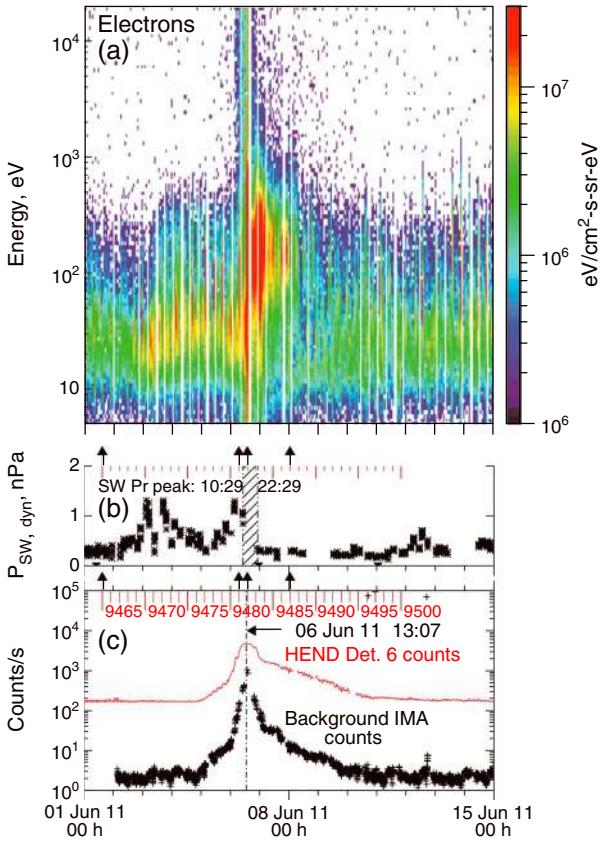

Figure 2. (a) Electron energy-time spectrogram from ASPERA-3/MEX covering the period of the ICME interaction with the Mars ionosphere. The color scale indicates differential energy flux; white vertical bands indicate no data. (b) Solar wind dynamic pressure derived from ASPERA-3 IMA proton measurements in the solar wind. The crosshatched region shows where IMA is incapacitated by the high fluxes. (c) ASPERA-3 IMA background counts (black) and Odyssey HEND charged particle counts (red). Both particle counts peak simultaneously around 13:00 UT on 6 June 2011 just prior to the periapsis pass of MARSIS AIS orbit 9482. The Mars Express orbit numbers are listed along the top axis. Upward pointing arrows in Figures 2b and 2c indicate the four orbits to be examined in greater detail.

logarithmically spaced energy steps between 10 eV and 36 keV with an energy resolution of 7% to measure the ions at a 12 s time resolution, using a 5.6° × 360° field of view. In this study, IMA achieves a 3-D field of view by an electrostatic sweep over 16 polar angles in 192 s (from −45° to 45° about the instrument plane). IMA measures the main components H^+, He^{2+}, He^+, O^+, and the molecular ions in the range $20 < m/q < 80$, where m and q are the ion mass and charge. The ions with different m/q are deflected differently by the magnet because the ion gyroradius depends on m/q, so that ions with different m/q hit the microchannel plate at different distances from the center of the instrument. A system of 16 anodes × 32 rings behind the microchannel plate records the radial position and the entrance angle of the ion hits. Since May 2007, measurements at energies below 50 eV are performed in 2-D, without the angular electrostatic sweep.

The High-Energy Neutron Detector, HEND, is one of three instruments that compose the Gamma Ray Spectrometer suite on board the Mars Odyssey spacecraft. The design of HEND, discussed in detail by *Boynton et al.* [2004], has six detectors for observing different energy ranges of neutrons. Detector 6 is the part of HEND that detects X-rays and charged particles for the purpose of anticoincidence rejection; however, here we use it for direct detection of charged particles.

3. Observations of the ICME Impact of 6 June 2011

3.1. Particle Observations With Mars Express ASPERA-3 and Odyssey HEND

At present, there is no solar wind monitor at Mars, a predicament that seriously impedes the study of space weather effects on the Martian ionosphere. It is hoped that this situation will be remedied in the near future. Until solar wind monitoring becomes a reality, Mars ionosphere researchers must be somewhat creative in timing and characterizing particle events at Mars. *Opgenoorth et al.* [2013] and the Mars Upper Atmosphere Network (MUAN) have handled the lack of a solar wind monitor by targeting Mars for intense observation during periods of conjunction between Mars and Earth. Observation of an event at Earth assists in tracing the progress of a space weather event originating at the Sun. In the current case, Mars and Earth were about 150° out of azimuthal alignment, and the relation with disturbances seen at Earth around the time of the event at Mars was not clear. This approach is therefore not open to us.

The ASPERA-3 instrument on MEX can be used to identify the interval between shock onset and end of the bulk plasma of the event. Figure 2a shows an energy-time spectrogram for solar wind/magnetosheath electrons observed by ASPERA-3 ELS over the course of the event in question, from undisturbed plasma beginning 1 June, through the peak disturbance on 6 June, to the moderately disturbed state on 15 June. To

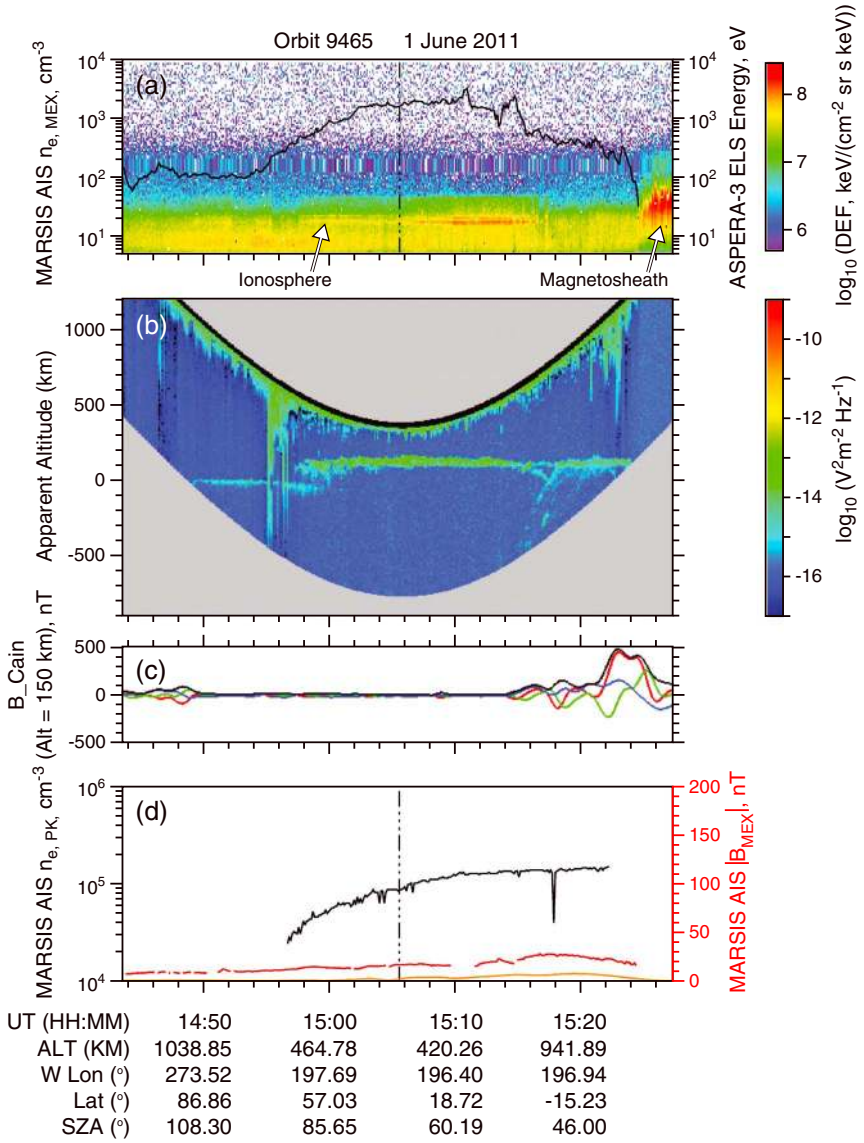

Figure 3. Summary ASPERA-3 ELS and MARSIS AIS data for 9465. This orbit represents a very quiet time preceding the onset of the ICME interaction with the Martian ionosphere. In this and the three following figures, the horizontal axis represents time, with corresponding spacecraft altitude, Mars west longitude, latitude, and solar zenith angle listed below. The data are given in four panels and are explained in the text.

complicate matters, there is a slight energization beginning on 3 June that appears to last through 6 June, which is probably unrelated to the large ICME that we wish to study.

Figure 2b shows the solar wind dynamic pressure computed from solar wind proton measurements made by IMA during the period under study. The dynamic pressure increases to values greater than 1 nPa between 3 and 4 June, coinciding with the small unidentified electron energization noted in Figure 2a. The dynamic pressure hits a minimum value of about 0.3 nPa on 5 June, then increases again. This increase is contiguous with a crosshatched region, seen in Figure 2b, representing a data gap in which IMA was incapacitated by extremely high energetic particle fluxes. The blackout of IMA particle data lasts for about 12 h starting ≈ 10:30 UT on 6 June and is seen to coincide closely with the energetic electron flux enhancement seen in Figure 2a.

Figure 2c shows data from two ion detection instruments. The ASPERA-3 IMA background, shown in black, corresponds to the counts recorded in the highest energy channels of IMA, caused by energetic particles

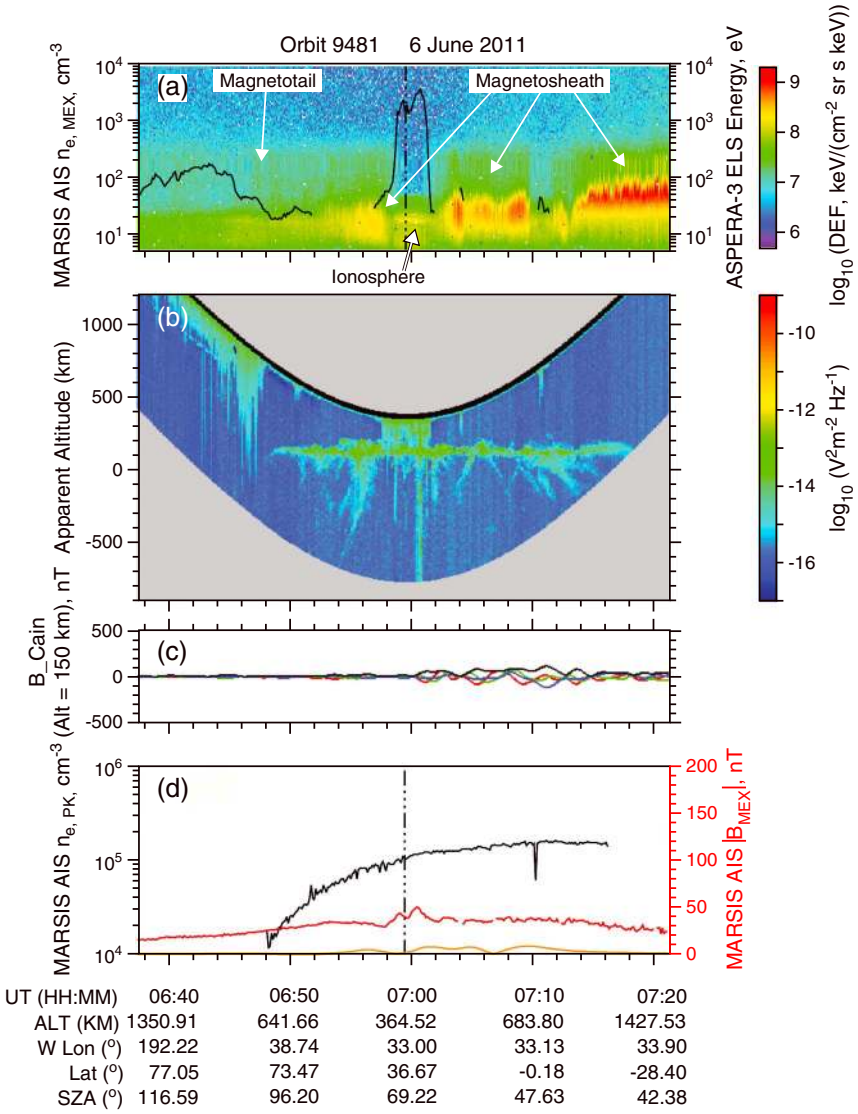

Figure 4. Summary ASPERA-3 ELS and MARSIS AIS data for orbit 9481, immediately preceding the ICME impact. All panels show the same quantities as in Figure 3, except that in Figure 4b the intensity is averaged between 1.0 and 2.5 MHz.

penetrating the instrument housing. (A similar method using ELS background was used by *Futaana et al.* [2008] to identify SEP events at Mars and Venus.) Detector 6 of HEND, shown in red, is a high-energy ion detector. Note that the peak of the HEND particle count coincides very well with the peak of the IMA background counts, implying that the source of the increase is global, consistent with an encompassing space weather event such as an ICME. The peak of the SEPs from these two detectors, simultaneous with orbit 9482, indicates that the ICME incorporates a shock, which encounters the Martian ionosphere around 10:30 UT of 6 June 2011. The MEX orbit numbers are shown in red at the top of Figures 2b and 2c, with arrows designating orbits to be especially considered.

The enhanced levels of SEPs indicated by the elevated IMA background and Odyssey HEND energetic particle counts peak around 13:00 UT of 6 June. The elevated SEPs are seen to coincide closely in time with both the high electron fluxes seen in Figure 2a and the blackout of IMA particles in Figure 2b. The start of this period of combined high fluxes in both ions and electrons, beginning around 10:30 UT on 6 June, immediately follows the solar wind dynamic pressure going above 1 nPa and is clearly the shock ahead of the ICME bulk plasma. After 22:30 UT, IMA is no longer incapacitated and the solar wind dynamic pressure is seen

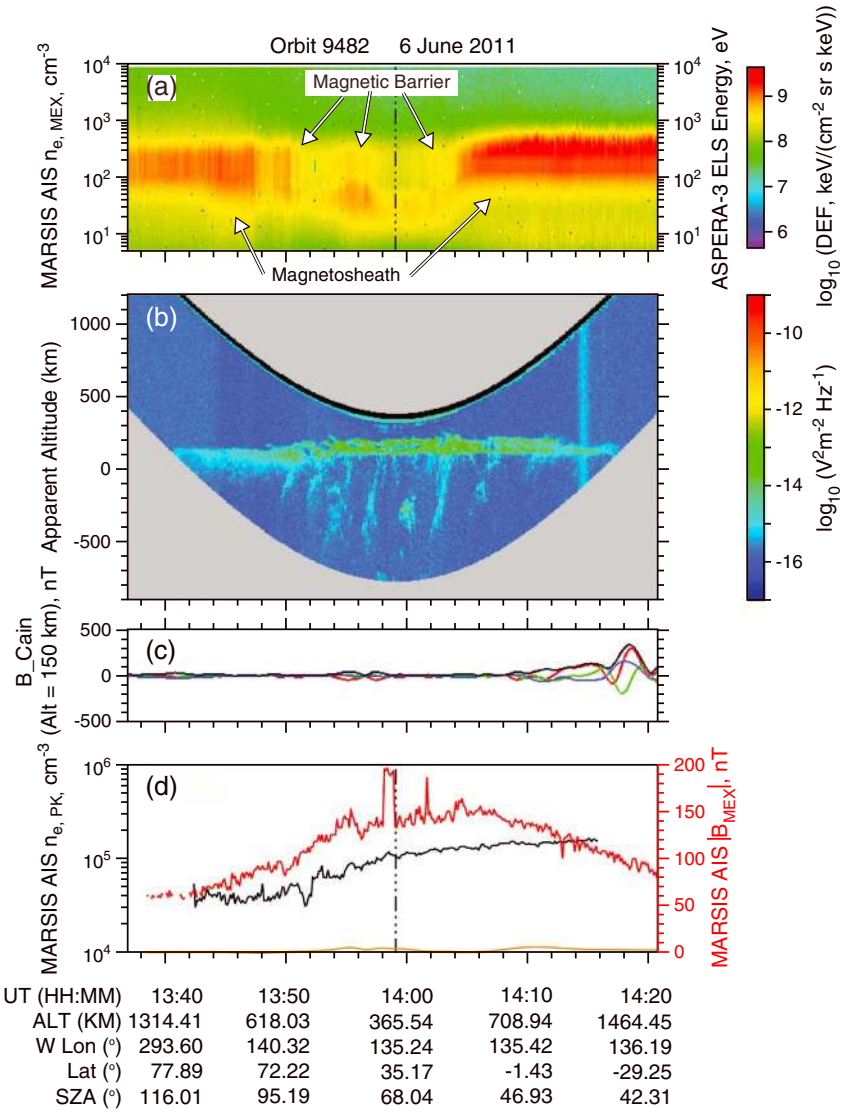

Figure 5. Summary ASPERA-3 ELS and MARSIS AIS data for 9482. This orbit occurs just after the ICME shock impacts the Martian ionosphere. All panels show the same quantities as in Figure 3, except that in Figure 5b the intensity is averaged between 1.0 and 2.5 MHz, and the color bar for the ASPERA-3 ELS flux is extended to higher values to avoid saturation.

to be steadily depressed to about 0.2 nPa until 13 June. The bulk plasma part of the ICME therefore must encounter the Martian ionosphere after the shock onset and during the IMA blackout. The SEPs drop sharply at about the time of IMA recovery and then further decline gradually until they return to their initial level on about 11 June. The enhanced SEPs during the ICME passage are consistent with longstanding observations of particles accelerated by interplanetary shocks [see, e.g., *Krimigis and Venkatesan*, 1988].

3.2. Selected Orbit Observations With MARSIS and ASPERA-3 ELS

In this section, we show time series of measurements taken by MARSIS AIS and ASPERA-3 ELS for the following orbits sampling various phases of the observed ICME encounter with the Martian ionosphere: orbit 9465, Figure 3 (quiet period well prior to impact); orbit 9481, Figure 4 (immediately prior to shock impact); orbit 9482, Figure 5 (immediately after the initial shock impact); and orbit 9487, Figure 6 (during recovery phase of the event). For reference, MEX orbit numbers are marked on Figure 2 with the four selected orbits marked with upward arrows.

Figures 3 through 6 all have the following format. The spacecraft altitude, Mars west longitude, latitude, and solar zenith angle are given with UT along the horizontal axis of each figure. Figure 3a shows the MARSIS

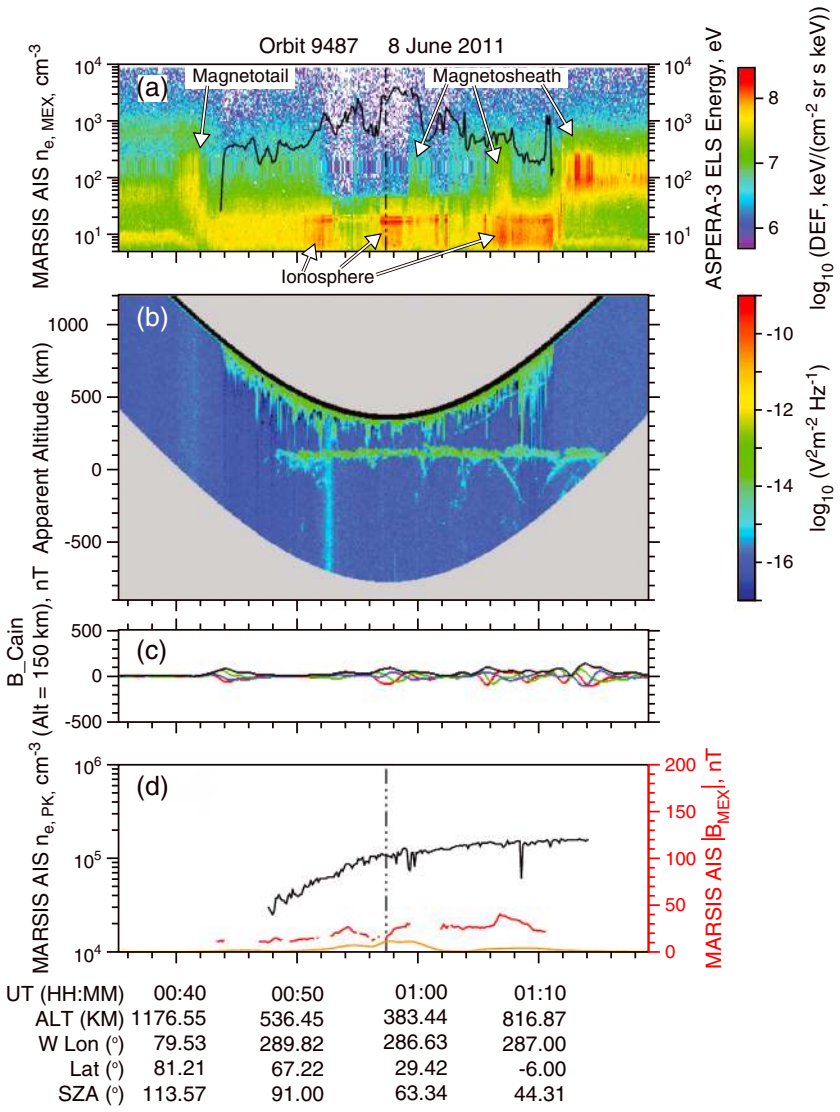

Figure 6. Summary ASPERA-3 ELS and MARSIS AIS data for 9487, during recovery from the ICME impact. All panels show the same quantities as in Figure 3.

local electron density plotted in black over the energy-time spectrogram of the omnidirectional differential electron flux from ASPERA-3 ELS. In these panels, the spacecraft is known to be in ionospheric plasma by the presence of strong, continuous 20–24 and 27 eV CO_2 photoelectron lines, while the magnetosheath plasma is identified by the presence of high fluxes of 40–100 eV electrons [*Frahm et al.*, 2006]. Figure 3b shows the simultaneous MARSIS radargram averaged between 1.5 and 2.5 MHz. In these panels, the vertical axis represents the apparent altitude, computed as the spacecraft altitude − the apparent range. The color coding gives the reflected intensity averaged for the given frequency range. The salient features are the surface reflection, at about 0 km apparent altitude, the ionospheric reflection, at about 130 km, and the hyperbollically shaped oblique echoes, with apices near or below the ionospheric reflection. Oblique echoes were originally identified and analyzed by *Gurnett et al.* [2005]. Subsequently they have been analyzed by *Duru et al.* [2006] and more recently by *Andrews et al.* [2014]. They are believed to represent irregularities in the ionosphere, usually near cusps in the crustal magnetic field. Figure 3c shows components and magnitude of the crustal magnetic field at 150 km altitude from the Mars crustal magnetic field model described by *Cain et al.* [2003], hereinafter "the Cain model." The red, blue, and green curves correspond to the radial, polar, and azimuthal components of the crustal field. Figure 3d shows the peak ionospheric electron density

from MARSIS (black), the MARSIS local magnetic field strength (red), and the Cain model field strength at the spacecraft (orange). Note that each panel is 45 min long and centered on that orbit's periapsis time. During the current mission phase, on a normal full pass MARSIS AIS operates up to a maximum altitude of 1550 km.

Figure 3 shows the MARSIS and ELS data from orbit 9465, which occur on 1 June 2011, well before the start of the event in question as well as before the weak event seen on 3–6 June. The ELS data in Figure 3a show that the MEX spacecraft is in the quiet ionosphere for almost the entire pass. MEX is seen to enter the magnetosheath at 15:24 UT, at which point the MARSIS AIS local electron density is seen to disappear. Figure 3b shows the robust surface reflection (the horizontal green line at 0 km apparent altitude) being replaced by the ionospheric reflection (horizontal green line at approximately 130 km apparent altitude) around 14:58 UT. Partial oblique echoes are seen at 15:18 UT. The short vertical green lines seen at the top of this panel are harmonics of the plasma frequency caused by the ringing of the plasma near the spacecraft in response to the MARSIS AIS sounding pulse. Figure 3c shows the components and magnitude of the crustal field at the spacecraft latitude and longitude at 150 km altitude. The oblique echoes in Figure 3b coincide with regions of elevated crustal magnetic field, shown in Figure 3c. This coincidence is consistent with the explanation of oblique echoes given by *Gurnett et al.* [2005], *Duru et al.* [2006], and *Andrews et al.* [2014]. Finally, in Figure 3d the peak ionospheric density varies smoothly, from the threshold of detection around 100° solar zenith angle (SZA) to a typical dayside value of 10^5 cm^{-3}. The measured magnetic field strength varies smoothly at low values a few times the local Cain field. This orbital pass was chosen as an example of a very quiet period. The three following figures, all in the same format, will show the Martian ionosphere in varying degrees of disturbance.

Figure 4 shows a stark contrast with the situation in Figure 3. In Figure 4a, the local plasma density drops abruptly from a maximum of 3×10^3 cm^{-3} to below the limit of detectability a few minutes on either side of periapsis. The disappearance of the local electron density is coincident with the intrusion of magnetosheath-like electrons at 06:52–06:57 UT and 07:03–07:10 UT. We interpret the disappearance of the local plasma density to mean that the outer boundary of the ionosphere has been compressed to altitudes below the spacecraft by the increasing solar wind dynamic pressure ahead of the ICME. During this period, MEX is in the magnetosheath, where the local electron density is not measurable due to high-speed plasma around the spacecraft [*Duru et al.*, 2008]. Where the local electron density is detectable, ionospheric photoelectron lines are clearly visible and higher-energy magnetosheath electrons, up to hundreds of electron volts, abruptly disappear. The local electron density exhibits two peaks around 07:00 UT, apparently an oscillation of the ionosphere. Figure 4b shows that the surface reflection has completely disappeared, the result of attenuation due to increased electron content in the ionosphere [see, for example, *Morgan et al.*, 2006; *Withers*, 2011]. This panel also reveals oblique echoes associated with low crustal fields before periapsis and moderate crustal fields after. Several of these oblique echoes are observed to occur simultaneously with the magnetosheath plasma intrusions, particularly the clear echoes with apex at 06:56 and 07:06UT. The ionospheric irregularities causing the oblique echoes are possibly explained by solar wind electron precipitation into magnetic cusp regions, with a possible increase in the neutral atmosphere scale height due to increased heating [see, e.g., *Gurnett et al.*, 2005]. The observations in this figure are consistent with this hypothesis, especially for the oblique echo with apex at 7:06 UT, where the modeled moderate crustal fields may allow for formation of open field lines. The local magnetic field seen in Figure 4d is slightly elevated over that from Figure 3, implying that the external magnetic is enhanced due to a rise in solar wind dynamic pressure as seen in Figure 2b. This mostly external magnetic field shows oscillation in unison with that of the electron density in Figure 4a. Note that this orbital pass begins at about 06:30 UT, just 4 h before the shock front hits MEX, as shown in Figure 2. If these oscillations are assumed to be temporal, they may be related to the global oscillations of the induced magnetosphere noted by *Futaana et al.* [2007] in response to an interplanetary shock at Mars. The profile of the peak ionospheric density is very similar to that in Figure 3.

The orbital pass featured in Figure 5 is radically different from the previous two orbits illustrated. MEX is now sampling the plasma about 3 h after the shock front hits MEX. In Figure 5a MARSIS AIS does not observe local plasma and the photoelectron lines are not seen. The ELS spectrogram is dominated by 100 eV electrons, indicating that MEX is in either the magnetosheath or magnetic barrier region and that the local plasma density is not measured by MARSIS in the fast, hot, tenuous flow [see, e.g., *Duru et al.*, 2008]. This occurs because the cold ionospheric plasma is pushed below the altitude of MEX by the increased solar wind dynamic pressure, seen in Figure 2b. Figure 5b indicates an ionospheric reflection between 0 and

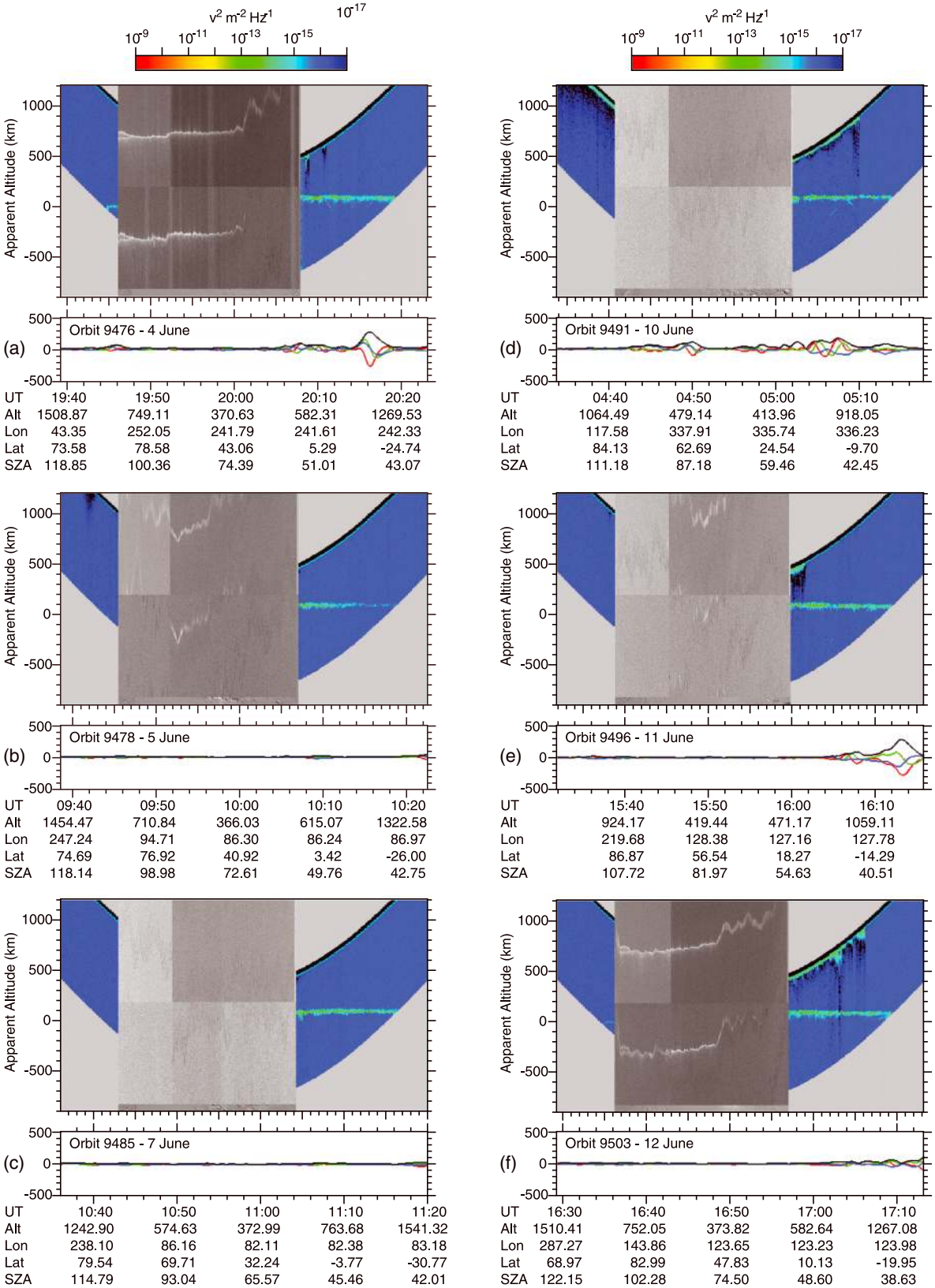

Figure 7. A series of six composite radargrams showing subsurface radar signal in two frequency bands surrounded by ionospheric mode echograms. Below the composite echograms, the crustal magnetic field components and magnitude are plotted with the same color convention as in Figure 3 and following. The data are for orbits (a) 9476, (b) 9478, (c) 9485, (d) 9491, (e) 9496, and (f) 9503.

130 km on the nightside: this low apparent altitude suggests that it could be oblique reflections from an extended transterminator ionosphere. Also, the surface reflection is not visible. Figure 5b also shows a series of oblique ionospheric echoes associated with low values of the crustal field, as indicated in Figure 5c. There are many diffuse and complex oblique echoes, several at negative apparent altitude. These echoes indicate oblique reflections from sources well away from the ground track of MEX. These intense and numerous echoes probably indicate an enhanced ionization and heating in magnetic cusps due to intense solar wind electron fluxes. Figure 5d indicates the magnetic field elevated to a steady 150 nT and briefly to 200 nT, although the crustal field is seen to be very small. This indicates a strong interplanetary magnetic field, as expected from the passage of an ICME. The large magnetic field strength typical of the ICME, coupled with the pressure pulse associated with the expected high plasma densities and possibly bulk velocities, contribute to make a strong external draped magnetic field on both dayside and nightside of Mars [*Crider et al.*, 2005]. Finally, the peak ionospheric density now does not drop off to below the detection threshold of 5000 cm^{-3}, reported by *Němec et al.* [2010], immediately at SZA of 100° as in Figures 3 and 4 but rather extends at high values to beyond SZA of 110°.

Finally, Figure 6a shows intermittent ionosphere punctuated with some higher-energy magnetosheath plasma. Figure 6b shows that the surface reflection has not yet returned but that the nightside "ionosphere" seen in Figure 5b is gone. The echogram in Figure 6b shows weak oblique echoes associated with moderate crustal fields in Figure 6c. Here the oblique echo with apex observed at 01:05 UT may be associated with ionization and heating by solar wind elecron entry, noted in Figure 6a, into the magnetic cusp, observed in Figure 6c. Figure 6d shows the magnetic field reduced to $<$ 50 nT and the peak ionosphere falling off below the MARSIS detection threshold as it approaches SZA of 100° consistent with orbits 9465 and 9481.

The picture that emerges, in the absence of IMA data during the most intense phase of the ICME impact, is that, just prior to the shock impact, rising solar wind dynamic pressure ahead of the ICME compresses and perhaps erodes the ionosphere to below the orbit of Mars Express, with some oscillations induced. Just after the shock, the magnetic field is dominated by the ICME field. Extra ionization caused by high fluxes of SEPs and by intense solar wind electron fluxes accompanying the shock may contribute, along with compression of the ionosphere, to increased peak ionospheric densities in the near-terminator nightside ionosphere [see, e.g., *Diéval et al.*, 2014; *Lillis and Brain*, 2013; *Němec et al.*, 2014]. These higher peak densities result in the extension of the detectable ionosphere well beyond the terminator. We shall further discuss this picture in section 4.

3.3. Combined MARSIS Subsurface and Ionospheric Sounding Signals During the ICME

As noted in section 2, the surface reflection from both MARSIS ionospheric and subsurface sounding modes is an indicator of the electron density of the ionosphere [*Morgan et al.*, 2006; *Espley et al.*, 2007; *Morgan et al.*, 2010]. As explained in *Morgan et al.* [2006], the surface reflection disappears because it is subject to collision damping as the electron density, electron temperature, and neutral density conspire to absorb the energy of the sounding wave. This effect has been quantified in detail by *Withers* [2011]; however, we here use it as a crude qualitative measure of departure of the electron density from typical values. This same process causes the disappearance of the surface reflection detected by the subsurface mode of MARSIS, as explained by *Espley et al.* [2007].

Because the dense ionospheric plasma on the dayside of Mars tends to obscure and distort the subsurface return signal, subsurface data tend to be taken on the nightside. On the nightside of Mars, therefore, most periapsis that pass below 850 km altitude are dedicated to subsurface mode, to the exclusion of topside ionospheric measurements. As noted by *Espley et al.* [2007], visibilities of surface reflection for the two modes are roughly congruent measures of the total electron density. In Figure 7 we show a series of six orbits worth of composite data covering the period of the ICME impact. The color bar and colored region are data from MARSIS AIS mode; the gray scale blocks of data are two frequency bands of MARSIS subsurface data. The panel below shows the Cain model crustal field at 150 km altitude, and ephemeris data are shown at the bottom of each part. In Figure 7a, for orbit 9476, one can see the surface reflection for about 2 min prior to the onset of the subsurface return. The surface reflection is visible in both subsurface and AIS modes. After the subsurface data are completed, around 20:08 UT, the ionospheric reflection is clearly visible, as it is in all subsequent examples. Referring to Figure 2, orbit 9476 is seen to be well before the shock passage of the ICME. In Figure 7b, orbit 9478, still before the shock, but in the region where SEPs are

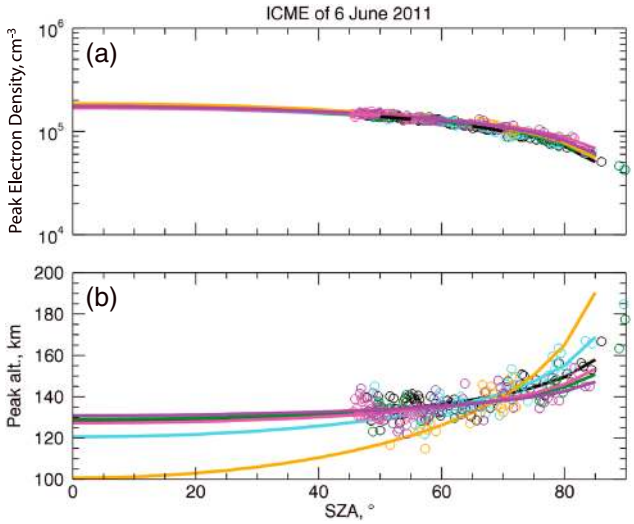

Figure 8. (a) Peak density of ionospheric traces as a function of solar zenith angle fit to a Chapman layer function for orbits 9465–black, 9467–cyan, 9475–green, 9481–orange, 9482–magenta, and 9487–violet. (b) Altitude of peak density as a function of solar zenith angle fit to a Chapman layer function color coded as in Figure 8a.

starting to increase, the surface reflection of the AIS mode has disappeared and the subsurface signal is more difficult to distinguish than previously. In Figures 7c and 7d, orbits 9485 and 9491, where Figure 2 indicates that the shock has passed but SEPs are still elevated, surface reflections from both modes are not visible. In Figure 7e, orbit 9496, where Figure 2c still shows a slight elevation in SEPs, the subsurface surface reflection has begun to reappear. Finally, in Figure 7f, orbit 9503, where the SEPs in Figure 2c have returned to their original level, the subsurface surface reflection is clearly visible; the AIS surface reflection is just visible between 16:34 and 16:36 UT. We see from this series of echograms that electron density remains elevated enough to diminish the intensity of the ionospheric surface reflection up to 6 days after the shock of the ICME has passed.

3.4. Peak Densities and Altitudes From AIS Remote Sensing

The AIS remote sounding ionospheric traces can be processed to give the actual electron density profile, a process that is discussed in detail by *Morgan et al.* [2008, 2013a, 2013b]. One way of analyzing these electron density profiles is to fit the peak densities and peak density altitudes to an ionospheric model. This was done by *Morgan et al.* [2008], using the Chapman layer model, in the form of equations (11) and (12) of that reference. Results of this procedure are shown in Figures 4–6 of *Morgan et al.* [2008], giving results for the subsolar ionospheric peak density, altitude of the subsolar peak density, and the neutral atmosphere scale height, assumed in the model to be a global constant. In the present work, we have followed a similar procedure using electron density profiles obtained for orbits 9465, 9467, 9475, 9481, 9482, and 9487, spanning the time of the ICME interaction with Mars. These profiles are fit, orbit by orbit, to a Chapman layer function as was previously done, with the addition that here we have fit to the exponent in the Chapman layer density equation, which is 0.5 for a true Chapman layer. Results of this fitting procedure are shown in Figure 8, where panels (a) and (b) show the peak electron density and the ionospheric peak altitude as a function of solar zenith angle. The output parameters are shown as a function of orbit number in Figure 9: (a) the quasi-Chapman exponent (canonically 1/2), (b) the neutral scale height, (c) the altitude of the subsolar ionospheric peak, and (d) the subsolar peak electron density. The results of these procedures are that orbit 9481, just prior to the shock and shown in orange in Figure 8, shows a significantly lower calculated subsolar

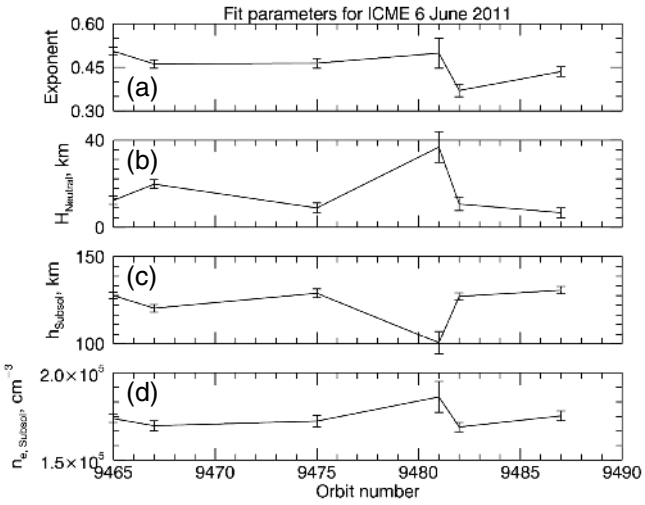

Figure 9. Results of Chapman layer fits for the same orbits as shown in Figure 8 as a function of orbit number. (a) Quasi-Chapman exponent. (b) Neutral scale height. (c) Altitude of subsolar peak density. (d) Subsolar peak density.

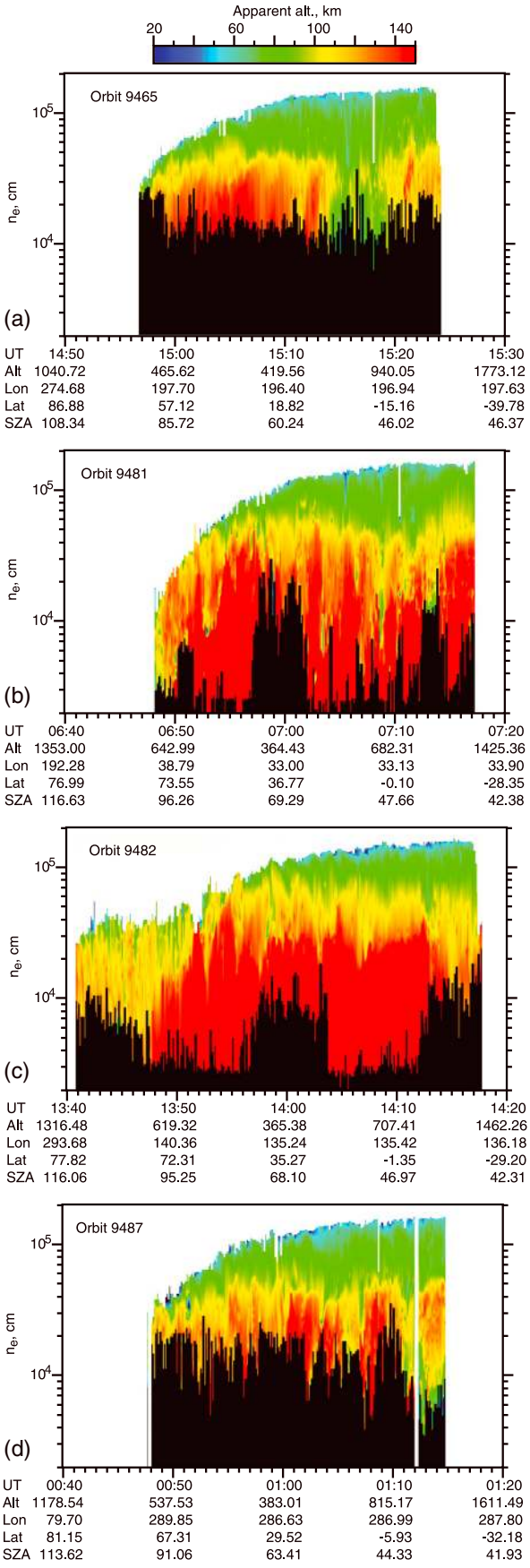

peak altitude than any of the other orbits while the corresponding subsolar peak density shows no significant change for the solar zenith angle range from 0 to 85°. This conclusion is quantified in Figure 9, which shows that orbit 9481 gives maxima in subsolar peak density, neutral scale height, and quasi-Chapman layer exponent, while showing the aforementioned minimum in subsolar peak altitude.

3.5. Apparent Altitudes of the Ionosphere During the ICME

Finally, we look at the remotely sensed ionospheric trace for the four full orbits detailed in Figures 3–6. An example of an ionospheric trace is labeled in the middle of Figure 1. The ionospheric trace is a profile of the delay time of the sounding wave as a function of the sounding frequency. As explained by *Morgan et al.* [2008, 2013b], and references therein [see, e.g., *Budden*, 1961; *Rishbeth and Garriott*, 1969], the delay time seen in an unprocessed ionogram is uncorrected for ionospheric dispersion and therefore cannot be thought of as an accurate representation of the ionospheric profile. It can, however, be used in a qualitative way to give an indication of ionospheric structure. As an example, *Kopf et al.* [2008] used spectrogram plots of the apparent altitude to explore the apparent upper layers in the Martian ionosphere. In Figure 10 we show spectrogram plots of the apparent altitude to show the effect of this ICME on the ionosphere as a whole. In these four plots, which show the same periapsis passes as Figures 3 through 6, the horizontal axis has UT and ephemeris data, the vertical axis shows electron density, and the color coding shows the apparent altitude scaled from each ionogram in the series, according to the color bar at the top. Black areas are low-density areas

Figure 10. This data format shows spectrograms of the apparent altitude as scaled from ionograms, as in Figure 1. The horizontal axis gives UT with ephemeris quantities; the vertical axis gives density; apparent altitude is color coded according to the color bar. (a) Orbit 9465, (b) orbit 9481, (c) orbit 9482, and (d) orbit 9487.

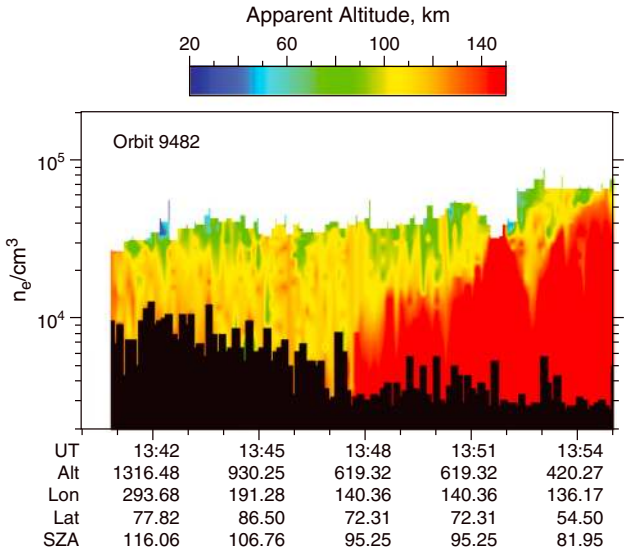

Figure 11. Blow up of Figure 10c, early part of the periapsis pass of orbit 9482 showing the wavelike and possibly turbulent structure of the transterminator extension of the ionosphere.

below the lowest-density reflection point for each ionogram. The result of these diagrams is a picture of the always changing nature of the Martian ionosphere. More specifically, this figure clearly shows the observed ionosphere in Figure 10c, for orbit 9482, extending to much higher solar zenith angles than for the other orbits. The tailward extension of the ionosphere agrees with the tailward extension shown in Figure 5c for the peak ionospheric frequency. In addition, in Figure 10c, we see that the extended region is in constant motion, with change on a very short time scale. Figure 11 is a blowup of the transterminator ionospheric extension from Figure 10c, showing the dynamic nature of the transterminator extension of the ionosphere. Figure 12 is an ionogram from the disturbed ionosphere of orbit 9482 showing that the ionosphere momentarily has three distinct layers and several oblique echoes. The closely spaced electron cyclotron echoes indicate that the magnetic field is extremely strong. Three distinct layers separated by cusps are shown in the ionogram. The cusps in apparent altitude indicate shelf-like or overhanging density structures, as discussed by *Kopf et al.* [2008]. In this case, the cusps and layers change on timescales of 7.5 s, the time resolution for ionograms. The rapid evolution of these layers and cusps indicate that the extended Mars ionosphere is undergoing wavelike or turbulent behavior.

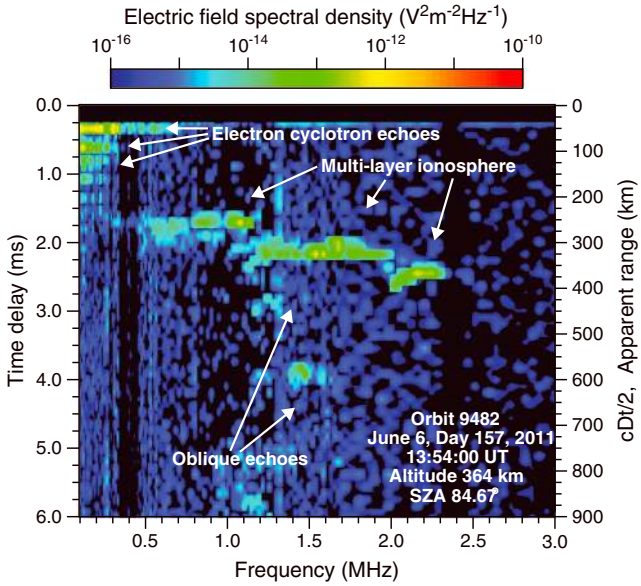

Figure 12. An ionogram from the disturbed ionosphere during orbit 9482. This ionogram shows closely spaced electron cyclotron echoes indicating the intense magnetic field. Three ionospheric layers are clearly seen as well as several oblique echoes at large delay times.

4. Interpretation

In June of 2011, a powerful ICME made a strong impact on the Martian ionosphere. We have shown in the preceding sections that the effects of this storm lasted over a week from pre-onset to full recovery. The peak of the particle data at Mars (Figure 2), indicating the passage of the shock associated with the ICME, has been seen to occur on 6 June, near midday, preceding the periapsis pass on orbit 9482 in topside sounding mode by less than an hour. Electron data from ASPERA-3 in Figure 2a show a slight energization of magnetosheath electrons starting on 3 June. This energization and a corresponding increase in solar wind dynamic pressure on 3 and 4 June are probably associated with a completely separate event; they are probably not relevant to the main event whose peak occurs on 6 June 2011 and which is associated with a solar wind dynamic pressure increase on 5 and 6 June.

Of the series of Figures 3–6, Figures 4 and 5 show a transition from a relatively quiet ionosphere to arrival and impact of the ICME, while Figure 6 shows characteristics of the recovery from the ICME impact. Figure 4 shows the MARSIS AIS and ASPERA-3 ELS picture of the ionosphere 5 or 6 h before peak impact. The ionosphere is seen to be compressed and probably eroded to a low altitude as seen from the observation of solar wind 100 eV electrons and the absence of observations of MARSIS local electron densities except near periapsis. ASPERA-3 outside the ionosphere detects entries of magnetosheath-like plasma that correspond to times when plasma from the transition region between the magnetosheath and ionosphere (aka magnetic pileup region) is pushed down to the spacecraft altitude by transient increases of the upstream dynamic pressure, in turn caused by ICME-related disturbances. The electron density local to MEX shows an increase from 100 to over 1000 cm^{-3} in a few minutes, immediately preceding MEX periapsis. For several minutes surrounding periapsis, photoelectron lines and MEX local electron densities are seen. This interval when MEX is clearly in the ionosphere is followed by an even faster decline in local electron density after periapsis, similar to ionopause-like events discussed by *Duru et al.* [2009]. The local plasma density undergoes what looks like an oscillation, a motion that is closely mimicked in the local magnetic field strength, shown in the same figure. We interpret this oscillation as a pulsation of the ionosphere under the rapidly rising pressure of the ICME similar to oscillations of the Martian system provoked by the passage of an interplanetary shock described by *Futaana et al.* [2007]. In addition, MARSIS sees an increased number of hyperbola-shaped oblique echoes that are not all associated with significant crustal magnetic field regions, contrary to the association that is usually observed, for example, by *Gurnett et al.* [2005], *Duru et al.* [2006], and *Němec et al.* [2011].

The next figure in the series, Figure 5 shows MARSIS and ASPERA-3 data about 3 h after shock onset at about 10:30 UT on 6 June. We have noticed that the local electron density is not visible in Figure 5a, signifying the compression and perhaps erosion of the ionosphere to altitudes below the orbit of the spacecraft. We have also taken note of the extremely intense and long-lived magnetic field strength that we believe to be associated with the ICME. The measurable ionospheric peak density now extends to SZA of 115°, whereas it usually drops below the MARSIS measurement threshold around an SZA of 100°, as seen in Figure 5 of *Gurnett et al.* [2008] as well as the present Figures 3, 4, and 6. We notice again the many oblique echoes with no association with strong crustal field regions.

The detection of the ionosphere up to solar zenith angle of 115° during the main ICME impact may be explained by an increased supply of plasma to the Martian nightside at that time. Several mechanisms may be involved: enhanced dayside-to-nightside plasma transport [*Fox et al.*, 1993], enhanced electron precipitation [*Lillis et al.*, 2011], enhanced solar energetic particle precipitation [*Němec et al.*, 2014]. We cannot use the IMA data here to support the hypothesis of plasma transport.

We know from MARSIS AIS data that there is a flow boundary around the ionosphere of Mars [*Duru et al.*, 2010]. This boundary separates the ionosphere from the more rapidly moving magnetosheath plasma. The ionospheric plasma is known to have a cross-terminator velocity of $\approx$ 5 km/s [*Fränz et al.*, 2010] during quiet times. We have seen that during the most intense phase of the ICME's impact with Mars, the Martian ionosphere is swept back across the terminator more strongly than usual, an indication that the ionospheric flow across the terminator boundary may be increased. There are indications that this flow is disturbed and possibly turbulent.

During this orbit, the large rise in the background counts of IMA and charged particle counts of HEND signals the peak of the SEP event at Mars, which contributes to the increase of the ionosphere electron density, as indicated by the disappearance of the ground trace in the echogram. Figure 7 demonstrates that enhanced ionospheric electron densities last for a considerable time after the impact, in this case about a week. The long-lived nature of the surface reflection disappearance has been noted previously by *Morgan et al.* [2006] and by *Espley et al.* [2007]; however, those authors did not have the timing of specific events to demarcate the interval. In this case we can see the impact directly. It is also worth noting that the disappearance of surface reflections begins on 5 June, the day preceding the ICME impact; the surface reflection was apparently unaffected by the smaller, unidentified, event on 3 and 4 June.

Oblique echoes indicate irregularities in the ionosphere that allow off-nadir reflections to be detected by the radar [see, e.g., *Gurnett et al.*, 2005; *Duru et al.*, 2006]. Open field lines with electron precipitation is a possible explanation for oblique echoes [*Němec et al.*, 2011]. Indeed we note that some of the apices of the oblique echoes identified in Figures 4 and 6 coincide with magnetosheath-like entries. Precipitation of 10–100 eV

electrons with sufficient fluxes to ionospheric altitudes into vertical magnetic fields might cause heating and ionization enough to increase the scale height, causing ionospheric irregularities and thus oblique echoes. More modeling of the precipitation process as well as reflection from the ionospheric irregularity is needed. Regardless of the detailed generation mechanism, our observations imply that the ICME impact causes violent oscillations in the magnetosheath-ionosphere boundary, causing the more numerous and complex oblique echoes. This interpretation is corroborated by the clear oscillatory motion seen in Figure 4, the rapidly changing ionosphere in Figure 11, and the clear, short-lived wavelike, multilayer structure in Figure 12.

Figures 8 and 9 show directly the effect of the ICME shock on the ionosphere. In accordance with Figure 2b, the sharp increase in dynamic pressure as the shock impinges on the ionosphere causes a compression that depresses the subsolar peak altitude of the main layer of the ionosphere from 130 km to 100 km altitude. The main layer returns to its normal altitude immediately after the shock impact, around the time of orbit 9482. Similarly, the neutral scale height peaks sharply immediately just before the shock impact, implying either compressional or collisional heating of the ionospheric plasma. The scale height reverts to normal values of approximately 10 km on orbit 9482. Finally, Figure 9a shows the "quasi-Chapman exponent" canonically a value of 0.5, dropping sharply on orbit 9482. This indicates a deviation from photochemical equilibrium, as one might expect in the aftermath of a shock passage. Figures 11 and 12 show the turbulent nature of the ionospheric plasma during this orbit, consistent with this picture of the shock impact.

5. Conclusions

We here list the primary effects reported in this study:

1. The shock associated with the ICME hits the Martian ionosphere at about 10:30 UT 6 June 2011. This is shown by a discontinuous enhancement of energetic electrons, dropout of the ion sensor on MEX, and increase in SEPs seen by IMA background and HEND charged particle detectors. Shock onset is about 4 h after the MARSIS data interval of MEX orbit 9481 and 3 h before MEX orbit 9482.
2. A strong compression of the ionosphere is evident on orbit 9481, just prior to the peak of the ICME impact.
3. Unison oscillations are apparent in the local ionospheric density and the magnetic field strength at this time indicating the likelihood of global oscillations of the Martian ionosphere caused by the sharp increase in solar wind dynamic pressure.
4. The subsolar peak altitude of the main layer of the ionosphere is compressed to 100 km from a normal value of approximately 130 km during orbit 9481.
5. ASPERA-3 IMA background counts and Odyssey HEND charged particle counts show that maximum SEP flux occurs near midday 6 June 2011, about 1.5 hours after the shock passage.
6. During orbit 9482, the local plasma frequency harmonics have disappeared, indicating that the MEX spacecraft is in the magnetosheath and the ionosphere is compressed and perhaps eroded below the orbit of Mars Express. At this time the magnetosheath was observed at lower altitudes than usual.
7. During this orbit remote sounding shows the main layer of the ionosphere to have recovered to its normal subsolar peak altitude of 130 km.
8. At the peak of the impact, during orbit 9482, the peak density of the ionosphere is detectable to SZA of $\sim 115°$, whereas during orbits occurring under quieter conditions, it is not clearly detected beyond SZAs of $\sim 100°$.
9. The transterminator extension of the ionosphere exhibited wavelike and perhaps turbulent motion.
10. During orbit 9482, 3 h after the shock impact, the local magnetic field strength is steadily about 150 nT and briefly as high as 200 nT, whereas it does not exceed 50 nT before and after the main impact. The magnetic field of the ICME is much greater than the local field.
11. The AIS mode surface reflection disappears by orbit 9478, about 1 day before the peak of the ICME impacts Mars on orbit 9482 and coinciding with the initial increase in SEPs seen by HEND and IMA. The subsurface mode surface reflection is partly obscured at this time. The subsurface mode surface reflection is partially recovered by orbit 9496, when SEPs are just returned to their base level. Both surface reflections have recovered by orbit 9503, about 1 week after the main phase of the ICME impacts Mars and after IMA and HEND SEP counts have returned to their base values.

To sum up, the shock impact causes a compression and oscillation of the ionosphere and an overwhelming increase in the magnetic field, which was evident in the MARSIS local electron density and magnetic field strength data. The measured ionospheric peak was extended to SZA of 115°, as opposed to its usual transterminator SZA limit of 100°. The enhanced ionospheric electron density due to the ICME impact began approximately 1 day before and lasted a week after the main ICME impact hit Mars. This ionization, evident in the attenuation of surface reflections is certainly due to SEPs and magnetosheath electrons both preceding and following the ICME impact. The extension of the remotely detectable ionosphere to SZA of 115° is evident only on orbit 9482. The wavelike or turbulent nature of the effect on the ionosphere was directly observed in the remotely sensed apparent altitude during the impact.

The nature of the extended ionosphere is left in question. The increase in attenuation due to high-energy particles in the environment implies that increased ionization must occur. The increased peak densities found at large solar zenith angle in orbit 9482 may due to ionization by large fluxes of SEPs and magnetosheath electrons. Also, the rapidly changing structure of the ionosphere, coupled with its very clear compression and relaxation, seems to imply that there is violent bulk motion of the ionospheric material, possibly including a strong transterminator flow. The relative importance of these two effects must be a subject of further inquiry.

The Mars Atmosphere and Volatile Evolution (MAVEN) spacecraft [*Jakosky and Maven Science Team*, 2008; *Lin and Jakosky*, 2012], to be inserted into Mars orbit in the fall of 2014, is completely dedicated to the study of the escape of matter from the Martian atmosphere. MAVEN carries two solar wind monitors and a magnetometer. MAVEN will also overlap with MEX, Odyssey, and other Mars missions, enabling monitoring of the solar wind while MEX and other spacecraft take data in the ionosphere. This combination of spacecraft will greatly improve our ability to explore the effects of ICMEs and other solar wind events on the atmosphere and ionosphere of Mars.

Acknowledgments
We acknowledge support from the International Space Science Institute (ISSI), Bern, CH, through the "Mars Induced Magnetosphere Team," led by M. Lester. Data from Mars Express MARSIS AIS and ASPERA-3 ELS and IMA are available from the NASA Planetary Data System (PDS) Geosciences Node. Data from Odyssey Gamma Ray Spectrometer, High-Energy Neutron Detector, are also available from the NASA PDS Geosciences Node. This work was completed under contract 1224107 administered by the Jet Propulsion Laboratory.

Masaki Fujimoto thanks the reviewers for their assistance in evaluating this paper.

References

Acuña, M. H., et al. (2001), Magnetic field of Mars: Summary of results from the aerobraking and mapping orbits, *J. Geophys. Res.*, *E10*, 23,403–23,417, doi:10.1029/2000JE001404.

Akalin, F., D. D. Morgan, D. A. Gurnett, D. L. Kirchner, D. A. Brain, R. Modolo, M. H. Acuña, and J. R. Espley (2010), Dayside induced magnetic field in the ionosphere of Mars, *Icarus*, *206*, 104–111, doi:10.1016/j.icarus.2009.03.021.

Andrews, D. J., H. J. Opgenoorth, N. J. T. Edberg, M. André, M. Fränz, E. Dubinin, F. Duru, D. D. Morgan, and O. Witasse (2013), Determination of local plasma densities with the MARSIS radar: Asymmetries in the high-altitude Martian ionosphere, *J. Geophys. Res. Space Physics*, *118*, 6228–6242, doi:10.1002/jgra.50593.

Andrews, D. J., H. J. Opgenoorth, N. J. T. Edberg, C. Diéval, F. Duru, D. A. Gurnett, D. D. Morgan, and O. G. Witasse (2014), Oblique reflection in the Mars Express MARSIS data set: Stable density structures in the Martian ionosphere, *J. Geophys. Res. Space Physics*, *119*, 3944–3960, doi:10.1002/2013JA019697.

Barabash, S., et al. (2004), ASPERA-3: Analyser of Space Plasmas and Energetic Ions for Mars Express, in *Mars Express: A European Mission to the Red Planet*, edited by A. Wilson, pp. 121–140, ESA Publications Division, ESTEC, Noordwijk, Netherlands.

Barabash, S., et al. (2006), The Analyzer of Space Plasmas and Energetic Atoms (ASPERA-3) for the Mars Express mission, *Space Science Rev.*, *126*, 113–164, doi:10.1007/s11214-006-9124-8.

Boynton, W. V., et al. (2004), The Mars Odyssey gamma-ray spectrometer instrument suite, *Space Sci. Rev.*, *110*, 37–83.

Budden, K. G. (1961), *Radio Waves in the Ionosphere*, Cambridge Univ. Press, Cambridge, U. K.

Cain, J. C., B. B. Ferguson, and D. Mozzoni (2003), An n = 90 internal potential function of the Martian crustal magnetic field, *J. Geophys. Res.*, *108*(E2), 5008, doi:10.1029/JE001487.

Committee on the Planetary Science Decadal Survey Space Studies Board (Eds.) (2011a), Chapter 3-Priority questions in planetary science for the next decade, in *Vision and Voyages for Planetary Science in the Decade 2013–2011*, pp. 3-1–3-20, The National Acad. Press, Washington, D. C.

Committee on the Planetary Science Decadal Survey Space Studies Board (Eds.) (2011b), Chapter 6-Mars: Evolution of an Earth-like world, in *Vision and Voyages for Planetary Science in the Decade 2013–2011*, pp. 6-1–6-41, The National Acad. Press, Washington, D. C.

Crider, D. H., D. Vignes, A. M. Krymskii, T. K. Breus, N. F. Ness, D. L. Mitchell, J. A. Slavin, and M. H. Acuña (2003), A proxy for determining solar wind dynamic pressure at Mars using Mars Global Surveyor data, *J. Geophys. Res.*, *108*(A12), 1461, doi:10.1029/2003JA009875.

Crider, D. H., J. Espley, D. A. Brain, D. L. Mitchell, J. E. P. Connerney, and M. H. Acuña (2005), Mars Global Surveyor observations of the Halloween 2003 solar superstorm's encounter with Mars, *J. Geophys. Res.*, *110*, A09S21, doi:10.1029/2004JA010881.

Diéval, C., D. D. Morgan, F. Němec, and D. A. Gurnett (2014), MARSIS observations of the Martian nightside ionosphere dependence on solar wind conditions, *J. Geophys. Res. Space Physics*, *119*, 4077–4093, doi:10.1002/2014JA019788.

Dubinin, E., M. Fränz, J. Woch, F. Duru, D. Gurnett, R. Modolo, S. Barabash, and R. Lundin (2009), Ionospheric storms on Mars: Impact of the corotating interaction region, *Geophys. Res. Lett.*, *36*, L01105, doi:10.1029/2008GL036559.

Dubinin, E., M. Fränz, A. Fedorov, R. Lundin, N. Edberg, F. Duru, and O. Vaisberg (2011), Ion energization and escape on Mars and Venus, *Space Sci. Rev.*, *162*, 173–211, doi:10.1007/s11214-011-9831-7.

Duru, F., D. A. Gurnett, T. F. Averkamp, D. L. Kirchner, R. L. Huff, A. M. Persoon, J. J. Plaut, and G. Picardi (2006), Magnetically controlled structures in the ionosphere of Mars, *J. Geophys. Res.*, *111*, A12204, doi:10.1029/2006JA011975.

Duru, F., D. A. Gurnett, D. D. Morgan, R. Modolo, A. F. Nagy, and D. Najib (2008), Electron densities in the upper ionosphere of Mars from the excitation of electron plasma oscillations, *J. Geophys. Res.*, *113*, A07302, doi:10.1029/2008JA013073.

Duru, F., D. A. Gurnett, R. A. Frahm, J. D. Winningham, D. D. Morgan, and G. G. Howes (2009), Steep, transient density gradients in the Martian ionosphere similar to the ionopause at Venus, *J. Geophys. Res.*, *114*, A12310, doi:10.1029/2009JA014711.

Duru, F., D. A. Gurnett, J. D. Winningham, R. A. Frahm, and R. Modolo (2010), A plasma flow velocity boundary at Mars from the disappearance of electron plasma oscillations, *Icarus*, *206*, 74–82, doi:10.1016/j.icarus.2009.04.012.

Edberg, N. J. T., H. Nilsson, A. O. Williams, M. Lester, S. E. Milan, S. W. H. Cowley, M. Fränz, S. Barabash, and Y. Futaana (2010), Pumping out the atmosphere of Mars through solar wind pressure pulses, *Geophys. Res. Lett.*, *37*, L03107, doi:10.1029/2009GL041814.

Espley, J. R., W. M. Farrell, D. A. Brain, D. D. Morgan, B. Cantor, J. J. Plaut, M. H. Acuña, and G. Picardi (2007), Absorption of MARSIS radar signals: Solar energetic particles and the daytime ionosphere, *Geophys. Res. Lett.*, *34*, L09101, doi:10.1029/2006GL0288.

Forbes, T. G., et al. (2006), CME theory and models, *Space Sci. Rev.*, *123*, 251–302, doi:10.1007/s11214-006-9019-8.

Fox, J. L., J. F. Brannon, and H. S. Porter (1993), Upper limits to the nightside ionosphere of Mars, *Geophys. Res. Lett.*, *20*, 1391–1394.

Frahm, R. A., et al. (2006), Carbon dioxide photoelectron energy peaks at Mars, *Icarus*, *182*, 371–382, doi:10.1016/j.icarus.2006.01.014.

Franklin, C. A., and M. A. Maclean (1969), The design of swept-frequency topside sounders, *Proc. IEEE*, *57*(6), 897–929.

Fränz, M., E. Dubinin, E. Nielsen, J. Woch, S. Barabash, R. Lundin, and A. Fedorov (2010), Transterminator ion flow in the Martian ionosphere, *Planet. Space Sci.*, *58*, 1442–1454, doi:10.1016/j.pss.2010.06.009.

Futaana, Y., S. Barabash, A. Grigoriev, D. Winningham, R. Frahm, M. Yamauchi, and R. Lundin (2007), Global response of Martian plasma environment to an interplanetary structure: From ENA and plasma observations at Mars, in *The Mars Plasma Environment*, edited by C. T. Russell, 315 pp., Springer-Verlag, New York, doi:10.1007/978-0-387-70943-7-12.

Futaana, Y., et al. (2008), Mars Express and Venus Express multi-point observations of geoeffective solar flare events in December 2006, *Planet. Space Sci.*, *56*, 873–880, doi:10.1016/j.pss.2007.10.014.

Gurnett, D. A., et al. (2005), Radar soundings of the ionosphere of Mars, *Science*, *310*, 1929–1933.

Gurnett, D. A., et al. (2008), An overview of radar soundings of the Martian ionosphere from the Mars Express spacecraft, *Adv. Space Res.*, *41*(9), 1335–1346, doi:10.1016/j.asr.2007.01.062.

Jakosky, B. M., and Maven Science Team (2008), The Mars Atmosphere and Volatile Evolution (MAVEN) Mars scout mission, *LPI Contributions*, *1447*, 9036.

Jordan, R., et al. (2009), The Mars Express MARSIS sounder instrument, *Planet. Space Sci.*, *57*, 1975–1986, doi:10.1016/j.pss.2009.09.016.

Kopf, A. J., D. A. Gurnett, D. D. Morgan, and D. L. Kirchner (2008), Transient layers in the topside ionosphere of Mars, *Geophys. Res. Lett.*, *35*, L17102, doi:10.1029/2008GL034948.

Krimigis, S. M. (1992), Voyager energetic particle observations at interplanetary shocks and upstream of planetary bow shocks—1977–1990, *Space Sci. Rev.*, *59*, 167–201, doi:10.1007/BF01262539.

Krimigis, S. M., and D. Venkatesan (1988), In situ acceleration and gradients of charged particles in the outer solar system observed by the Voyager spacecraft, *Astrophys. Space Sci.*, *144*, 463–486, doi:10.1007/BF00793199.

Lillis, R. J., and D. A. Brain (2013), Nightside electron precipitation at Mars: Geographic variability and dependence on solar wind conditions, *J. Geophys. Res. Space Physics*, *118*, 3546–3556, doi:10.1002/jgra.50171.

Lillis, R. J., M. O. Fillingim, and D. A. Brain (2011), Three-dimensional structure of the Martian nightside ionosphere: Predicted rates of impact ionization from Mars Global Surveyor magnetometer and electron reflectometer measurements of precipitation electrons, *J. Geophys. Res.*, *116*, A12317, doi:10.1029/2011JA016982.

Lin, R. P., and B. Jakosky (2012), The 2013 Mars Atmosphere and Volatile Evolution (MAVEN) mission to Mars, in *39th COSPAR. Scientific Assembly. Vol. 39 of COSPAR Meeting*, p. 1089, abstract PSB.1-23-12.

Lundin, R., S. Barabash, M. Holmström, H. Nilsson, M. Yamauchi, M. Fränz, and E. M. Dubinin (2008), A comet-like escape of ionospheric plasma from Mars, *Geophys. Res. Lett.*, *35*, L18203, doi:10.1029/2008GL034811.

Lundin, R., S. Barabash, M. Holmström, H. Nilsson, M. Yamauchi, E. M. Dubinin, and M. Fränz (2009), Atmospheric origin of cold ion escape from Mars, *Geophys. Res. Lett.*, *36*, L17202, doi:10.1029/2009GL039341.

McEnulty, T. R., J. G. Luhmann, I. de Pater, D. A. Brain, A. Fedorov, T. L. Zhang, and E. Dubinin (2010), Interplanetary coronal mass ejection influence on high energy pick-up ions at Venus, *Planet. Space Sci.*, *58*, 1784–1791, doi:10.1016/j//pss.2010.07.019.

Morgan, D. D., D. A. Gurnett, D. L. Kirchner, R. L. Huff, D. A. Brain, W. V. Boynton, M. H. Acuña, J. J. Plaut, and G. Picardi (2006), Solar control of radar wave absorption by the Martian ionosphere, *Geophys. Res. Lett.*, *33*, L13202, doi:10.1029/2006GL026637.

Morgan, D. D., D. A. Gurnett, D. L. Kirchner, J. L. Fox, E. Nielsen, and J. J. Plaut (2008), Variation of the Martian ionospheric electron density from Mars Express radar soundings, *J. Geophys. Res.*, *113*, A09303, doi:10.1029/2008JA013313.

Morgan, D. D., et al. (2010), Radar absorption due to a corotating interaction region encounter with Mars detected by MARSIS, *Icarus*, *206*, 95–103, doi:10.1016/j.icarus.2009.03.008.

Morgan, D. D., O. Witasse, E. Nielsen, D. A. Gurnett, F. Duru, and D. L. Kirchner (2013a), The processing of electron density profiles from the Mars Express MARSIS topside sounder, *Radio Sci.*, *48*(3), 197–207, doi:10.1002/rds.20023.

Morgan, D. D., D. A. Gurnett, D. L. Kirchner, J. L. Fox, E. Nielsen, and J. J. Plaut (2013b), Correction to "Variation of the Martian ionospheric electron density from Mars Express radar soundings", *J. Geophys. Res. Space Physics*, *118*, 4710, doi:10.1002/jgra.50369.

Němec, F., D. D. Morgan, D. A. Gurnett, and F. Duru (2010), Nightside ionosphere of Mars: Radar soundings by the Mars Express spacecraft, *J. Geophys. Res.*, *115*, E12009, doi:10.1029/2010JE003663.

Němec, F., D. D. Morgan, D. A. Gurnett, and D. A. Brain (2011), Areas of enhanced ionization in the deep nightside ionosphere of Mars, *J. Geophys. Res.*, *116*, E06006, doi:10.1029/2011JE003804.

Němec, F., D. D. Morgan, C. Diéval, D. A. Gurnett, and Y. Futaana (2014), Enhanced ionization of the Martian nightside ionosphere during solar energetic particle events, *Geophys. Res. Lett.*, *41*, 793–798, doi:10.1002/2013GL058895.

Opgenoorth, H. J., D. J. Andrews, M. Fränz, M. Lester, N. J. T. Edberg, D. Morgan, F. Duru, O. Witasse, and A. O. Williams (2013), Mars ionospheric response to solar wind variability, *J. Geophys. Res. Space Physics*, *118*, 6558–6587, doi:10.1002/jgra.50537.

Picardi, G., et al. (2004), MARSIS: Mars Advanced Radar for Subsurface and Ionosphere Sounding, in *Mars Express: A European Mission to the Red Planet*, edited by A. Wilson, pp. 51–69, ESA Publications Division, ESTEC, Noordwijk, Netherlands.

Rishbeth, H., and O. K. Garriott (1969), *Introduction to Ionospheric Physics*, 331 pp., Academic Press, New York.

Sarris, E. T., and J. A. V. Allen (1974), Effects of interplanetary shock waves on energetic charged particles, *J. Geophys. Res.*, *79*, 4157–4173.

Uluşen, D., D. A. Brain, J. G. Luhmann, and D. L. L. Mitchell (2012), Investigation of Mars' ionospheric response to solar energetic particle events, *J. Geophys. Res.*, *117*, A12306, doi:10.1029/2012JA017671.

Vourlidas, A., B. J. Lynch, R. A. Howard, and Y. Li (2013), How many CMEs have flux ropes? Deciphering the signatures of shocks, flux ropes, and prominences in coronagraph observations of CMEs, *Sol. Phys.*, *284*, 179–201, doi:10.1007/s11207-012-0084-8.

Withers, P. (2011), Attenuation of radio signals by the ionosphere of Mars: Theoretical development and application to MARSIS observations, *Radio Sci.*, *46*, RS2004, doi:10.1029/2010RS004450.